Surface functionalization with nanostructure patterning by a green nanosecond pulsed laser

WCMNM 2021

Themistoklis Karkantonis[1], Anvesh Gaddam[1], Tian Long See[2], Stefan Dimov[1]

[1] *Department of Mechanical Engineering, University of Birmingham, Birmingham, B15 2TT, UK*
[2] *The Manufacturing Technology Centre Ltd, Coventry, CV7 9JU, UK*

Abstract

Laser-induced periodic surface structures (LIPSS) are nanometric surface undulations produced by short and ultrashort pulsed lasers. However, when nanosecond pulsed lasers are employed, the thermal processing could result in surface oxidation and subsequent deterioration of LIPSS. In this work, the LIPSS were fabricated by a nanosecond green laser operating under ambient and argon environments to investigate the quality of LIPSS on stainless steel surfaces. The LIPSS quality was correlated to the diffracted light intensity and their key parameters such as periodicity and amplitude. The LIPSS formation was observed at an accumulated fluence of above 13.85 J/cm^2 and the optimal processing window was sustained up to 46.17 J/cm^2 before the oxidation occurred. LIPSS generated in the argon environment had a higher intensity of the diffracted light, exhibiting minimal surface oxidation according to XPS analysis and had a high amplitude ripples than those in the air. The results reported provide insights into the influence of ambient conditions on LIPSS generated with nanosecond green lasers.

Keywords: Argon, fluence, LIPSS, nanosecond, oxidation, XPS.

1. Introduction

Laser-induced periodic surface structures (LIPSS) are periodical ripple-like nanostructures which can be imprinted on a variety of materials by employing linearly polarized laser sources [1]. These surface structures can be clustered into low spatial frequency LIPSS (LSFL) and high spatial frequency LIPSS (HSFL) with periodicities close to and much smaller than the laser wavelength, respectively. Among them, only LSFL, referred to as LIPSS in this research, can be obtained both with ultra-short (fs and ps) and longer (≥ ns) pulse durations and have attracted more attention from researchers [2]. Owing to their wide applicability and varying geometrical characteristics, these ripple-like structures have been extensively investigated as a means for functional surface treatments. More specifically, surfaces textured with such nanoscale ripples have displayed superhydrophobic [3], anti-bacterial [4], anti-icing [5], and cell-adhesion [6] properties in applications related to food packaging, biomedical and energy storage sectors.

To imprint all these attractive functionalities, it is of great importance to generate uniform and homogeneous LIPSS on the processed materials. At present, most studies have been focused on the use of ultra-short pulsed lasers to attain uniform LIPSS onto the surface. Although, high precision, controllability and minimum heat affected zone (HAZ) can be achieved by employing ultrashort lasers, their average power is relatively low and consequently this entails longer processing times. On the contrary, nanosecond lasers are a cost-effective alternative to treat large surface areas without requiring substantial investments. One of the main concerns when employing lasers with longer pulse durations for texturing/structuring metallic surfaces is that this is thermal processing with the associated heat-induced negative side effects, i.e. oxidation and re-cast formations on the surface. Nevertheless, the level of laser-induced oxidation can be minimized upon irradiation in a controlled argon environment [7].

In general, the use of nanosecond lasers on metals has been mostly limited to the creation of superhydrophobic surfaces by taking advantage of their negative side effects, i.e. by roughening the surface [8] or the fabrication of LIPSS when operating at near-infrared wavelengths [9]. Although, the importance of this technology for functionalizing surfaces at an industrial level is recognized through these studies, few publications were focused on investigating the generation of LIPSS on metallic substrates [10,11]. Thus, it is clear that further efforts are necessary to quantitatively evaluate the LIPSS formation with nanosecond lasers, especially their impact on metallic surfaces when the processing is performed in different controlled environments. At the same time, the functional response of such laser-induced sub-wavelength surface structures that can be generated with green nanosecond lasers were not sufficiently explored whilst they are important for developing new application areas for this technology.

This research reports an investigation into the formation, evolution and properties of LIPSS generated with a green nanosecond pulsed laser on stainless steel substrates in different gas environments. A simple one-step texturing routine was implemented to study the evolution of LIPSS over large areas. Homogenous LIPSS with intense light diffraction are formed in both atmospheric and argon gas environment, whilst the impact on surface chemistry is studied.

2. Materials and methods

2.1 Experimental set up and process parameters

Commercially available AISI 316 stainless steel (SS) rectangular plates with a 0.5 mm thickness and an average roughness (S_a) of 30 nm were used in the LST experiments. The experiments were conducted on the state-of-the-art LASEA LS4 laser micro-machining workstation. The platform integrates a s-polarized nanosecond fiber laser source (GLPN -500-1.5-50-M, IPG) with a maximum average power of 50 W, which delivers a pulse duration of 1.5 ns at a nominal wavelength of 515 nm. A scan head (LS-Scan XY 20) is used to steer the laser beam across the samples at a maximum scanning speed of 2 m/s. A

telecentric lens with 100 mm focal distance was utilized to focus the laser beam down to a spot size ($2w_0$) of 40 μm at the focal plane. Thereafter, the accurate positioning of the samples at the focal plane was performed using three linear motorized stages in combination with a high-resolution positioning camera (Dino-Lite Premier, AM7013MT).

The SS substrates were textured by using a horizontal raster scanning strategy, in which a constant hatch distance (h) of 1 μm was set between two consecutive beam scan lines. To study the generation and evolution of LIPSS onto the surface, the laser texturing was carried out at various scanning speeds (v) from 0.3 to 2 m/s and average power (P) between 0.189 and 0.671 W. At the same time, the pulse repetition rate (f) was fixed at 100 kHZ during the experimental trials. The pulse-to-pulse distance ($d = v/f$) along the scanning direction and the pulse fluence (F_0) were determined, and then used for calculating the effective number of pulses per unit area (N_{eff}) and the effective accumulated fluence per unit area (F_{acc}) based on the expressions presented in [12], in particular:

$$N_{eff} = \frac{\pi w_0^2}{dh} \quad (1)$$

$$F_{acc} = N_{eff} F_0 = \frac{P}{fdh} \quad (2)$$

Furthermore, the same experimental procedure was repeated under atmospheric and argon gas environments to investigate their impact on surface morphology or chemical state after undergoing LIPSS treatments. The laser texturing of samples in a controlled argon gas environment were conducted inside a hollow cylindrical aluminum chamber. As argon is heavier compared to air, the SS samples were placed at the bottom of the chamber while the gas filled the enclosed area at a constant flow rate of 12 L/min.

2.2 Surface characterization techniques

The surface topographies of the textured SS substrates were initially characterized using a tabletop Scanning Electron Microscope (SEM, Hitachi TEM3030Plus). To capture the first order diffracted light out of the treated surfaces, an optical microscope (Alicona G5) was employed by holding a collimated white light beam at an incident angle of 60° relative to the sample surface. An open-source image analysis software (ImageJ) was used to extract the mean light intensity of the signal. The morphology of the nanoscale topographies was captured by using Atomic Force Microscopy (AFM, MFP-3D, Asylum Research, USA) together with 2D Fast Fourier Transformation (FFT) analysis to evaluate their spatial periods. The acquired scan images were analyzed using an open-source image analysis software (Gwyddion).

To inspect the surface chemistry of the substrates produced under air and argon gas environments, a X-ray Photon Spectroscopy (XPS) was conducted by using a Kratos Axis SUPRA spectrometer. The survey scans in the range of 0 to 1200 eV binding energy were recorded at pass energies of 160 eV, whilst the high-resolution ones at pass energies of 40 eV. The step sizes were 1 eV and 0.1 eV, respectively. The curve fitting was implemented in CasaXPS using a Shirley type for background subtraction.

The wetting properties of the treated surfaces were assessed with a goniometer (OCA 15EC, Data Physics GmbH, Germany). More specifically, water droplets of 4 μl were dispersed on the surface and the corresponding static contact angle values were recorded.

3. Results and discussion

3.1 LIPSS evolution in ambient environment

The primary goal was to identify the minimum accumulated fluence required for LIPSS generation on the irradiated surface using a single pass laser process when operating at high processing speeds, which is a key aspect for their broader implementation in industrial applications. As can be seen in Fig. 1, the accumulated fluence threshold for LIPSS generation at a scanning speed of 2 m/s was determined to be as low as 13.85 J/cm^2.

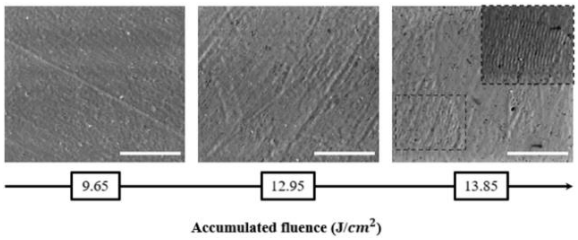

Fig. 1. Evolution of LIPSS over large areas with the increase of accumulated fluence at a scanning speed of 2 m/s (scale bar: 10 μm).

Thereafter, the irradiation of SS samples was conducted above the predetermined LIPSS threshold with varied pulse fluence and fixed number of pulses. Three representative SEM images of LIPSS as a result of the increasing pulse fluence but the same beam overlap of 75 % are provided in Fig. 2a, whilst their corresponding first order diffracted light intensity are provided in Fig. 2b. For normal beam incidence angle, the orientation of LIPSS was found to be perpendicular to the laser polarisation. At the early stage of LIPSS generation, some pits/holes were observed on the surface which gradually almost disappeared as the pulse fluence was further increased. The formation of these surface defects may be attributed to some low-level heating and consequently not well pronounced melting of the material. By increasing further the pulse fluence, more consistent and pronounce LIPSS formed on the surface that resulted in a higher diffracted light intensity. Overall, it is worth stating that the accumulated fluence for LIPSS generation with the green nanosecond laser was identified to be in the range from 13.85 to 46.17 J/cm^2.

Furthermore, the influence of overlap between two successive pulses on the evolution of LIPSS was also analysed. The representative SEM micrographs in Fig 3a and c depict LIPSS topographies generated with pulse fluences of 150.48 and 171.18 mJ/cm^2 but with different overlapping values, respectively. As the distance between two successive pulses decreased, the necessary pulse fluence to produce regular LIPSS was significantly decreased, too. This phenomenon is associated with the material dependent incubation effect, which leads to a reduction in the material's ablation threshold when the number of pulses per spot increases. In addition, an optimum beam overlap exists for obtaining highly uniform LIPSS onto the irradiated material. Considering LIPSS topographies

together with their corresponding light diffraction responses in Fig. 3 b and d, an overlap factor of 85 % had proved advantageous for efficient LIPSS generation.

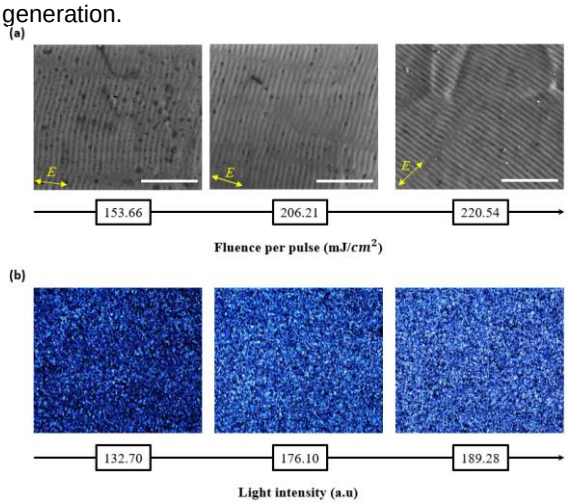

Figure 2. The LIPSS evolution with an increasing pulse fluence and constant pulse to pulse distance of 10 µm: (a) the SEM micrographs of textured surfaces (scale bar: 5 µm); (b) the corresponding first order light diffraction of LIPSS treated surfaces in (a).

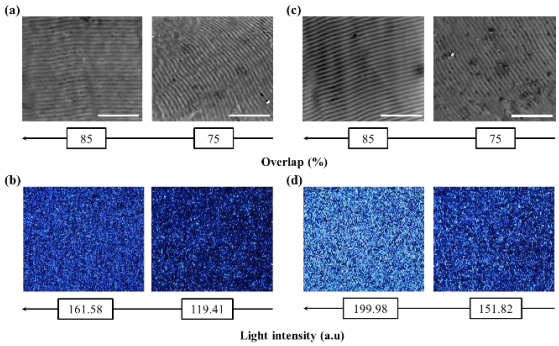

Fig. 3. The LIPSS formation with two different pulse overlaps and their corresponding diffracted light intensity: (a-b) pulse fluence of 150.48 mJ/cm^2; (c-d) pulse fluence of 171.18 mJ/cm^2. (scale bar: 5 µm).

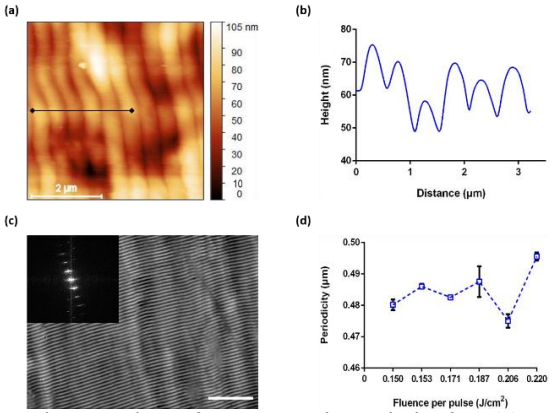

Figure 4. The surface topography analysis of LIPSS substrates: (a) the AFM micrograph showing LIPSS fabricated with accumulated fluence of 35.83 J/cm^2 and overlap of 85 %; (b) the LIPSS profile as extracted from the AFM measurements; (c) the SEM micrograph with a 2D FFT image inset in. (scale bar: 5 µm); (d) the evolution of LIPSS spatial periodicities with the increase of pulse fluence.

Representative AFM and SEM images of the most highly regular LIPSS fabricated with an accumulated fluence of 35.83 J/cm^2 are provided in Fig. 4a and c, respectively. The extracted surface profile in Fig. 4b shows LIPSS average height obtained perpendicular to their orientation. From all the analysed LIPSS, it was revealed that there was a positive correlation between these structures' amplitude and the applied accumulated fluence (up to a certain extent). For an accumulated fluence of 35.83 J/cm^2, the LIPSS height was in the range of 9.15 - 21.14 nm (peak to valley distance). As can be seen in Fig 4d, the main spatial periodicities of LIPSS topographies were below the laser wavelength and varied between 473 and 498 nm based on the applied pulse fluence.

3.2 LIPSS evolution in argon gas environment

The optimum laser processing parameters, i.e. overlap of 85 %, were used to compare the evolution of LIPSS when laser texturing was conducted in argon gas. The SEM micrographs in Fig. 5a and b depict the LIPSS topographies fabricated with pulse fluences of 150.48 and 171.18 mJ/cm^2, respectively. As can be seen, the LIPSS quality varied with the pulse fluence. The optimum conditions for uniform LIPSS formation in argon gas was achieved at a pulse fluence of 150.48 mJ/cm^2, where minimum surface defects were observed. The surface profiles (see Fig. 5c and d) of the LIPSS produced with identical laser process settings in argon to those in ambient air show a mean LIPSS height of 24.23 ± 2.97 nm and 8.28 ± 3.07 nm, respectively. Therefore, it is evident that LIPSS formed under irradiation in argon gas can achieve higher amplitudes.

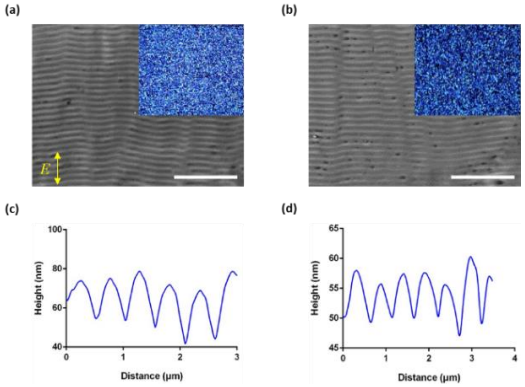

Fig. 5 The surface topography analysis of LIPSS treated substrates: (a-b) the SEM micrographs showing LIPSS fabricated in argon with a laser beam overlap of 85 % and pulse fluence of 150.48 and 171.18 mJ/cm^2, respectively, with diffracted light images insert in. (scale bar: 5 µm); (c-d) the surface profiles showing average height of LIPSS produced with an accumulated fluence of 31.50 J/cm^2 under argon and ambient conditions, respectively.

3.3 Surface chemistry analysis

XPS analysis was conducted to investigate the alterations in surface chemistry after the LIPSS generation in both argon and air gas environment. Table 1 presents the surface chemical compositions of the untreated SS substrate and the LIPSS ones processed with accumulated fluences of 31.50 and 35.83 J/cm^2, namely (LIPSS-I, LIPSS-II), in argon and ambient air conditions, respectively.

The elemental composition of the untreated SS surface is characterized by higher concentration of carbon compared to oxygen and significantly low amount of metals. The detection of non-zero carbon is mainly associated with the adsorption of organic matters from the atmosphere. On the other hand, the

oxygen content increased together with that of Fe and Cr on the surfaces subjected to a laser treatment. Based on these findings, it can be judged that the LIPSS generation led to the exposure of more Fe and Cr from the bulk to the ambient air, which instantly reacted and formed a mixed oxide layer at the surface. However, it should be emphasized that the values of O/Fe and O/Cr ratios decreased dramatically on these surfaces in comparison to the untreated one, especially after irradiation in controlled argon gas environment. By analyzing the Fe2p spectrum, the Fe (III) oxide state dominate on all the surfaces. Nevertheless, it should be highlighted that the samples processed in argon gas had some contribution of pure metallic components. These results are consistent with the calculated indirect ratios that are provided in Table 1. Thus, they confirm the capabilities of LIPSS treatments in controlled argon gas to generate highly uniform LIPSS with minimum laser-induced oxidation as a side effect on the surface.

Table 1
Elemental composition extracted from the XPS survey spectra of untreated and laser processed SS surfaces.

Surface	C (at%)	O (at%)	Fe (at%)	Cr (at%)	O/Fe	O/Cr
Untreated	59.95	35.00	3.50	1.55	10.00	22.58
LIPSS-I (argon)	37.02	46.75	8.64	7.59	5.41	6.16
LIPSS-I (air)	44.33	44.62	6.00	5.05	7.44	8.84
LIPSS-II (argon)	35.05	48.18	10.26	6.51	4.70	7.40
LIPSS-II (air)	45.00	42.79	7.52	4.69	5.69	9.12

.

3.4 Contact angle analysis

The wetting properties of the LIPSS surfaces produced in air and argon environments were investigated to understand the influence of surface chemistry and topography on contact angles (see Fig. 6). It is apparent that the contact angle decreased immediately after the LIPSS treatment in air and argon environments. This reduction is more pronounced on the samples processed in argon. On these surfaces, the decomposition of CO_2 favors the formation of Fe_3O_4 and the surface becomes rich in oxygen-to-carbon ratio over a period of time. For instance, the O/C on such samples is 1.2 - 1.3, whereas on the ones treated in air is 0.9 - 1.0. At the same time, the LIPSS are deeper in the samples processed in argon than those in air. Therefore, the combined effects of topography and surface chemistry led to an increase in the contact angle on LIPSS generated in argon environment.

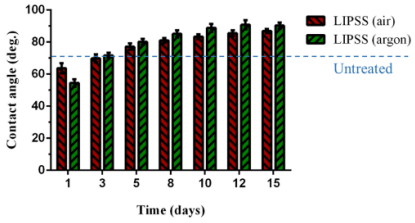

Fig. 6 Contact angle evolution as a function of time in number of days on untreated and LIPSS treated substrates in the air and argon environments.

4. Conclusions

The generation of homogeneous LIPSS cost-effectively on relatively large surfaces is an important step towards toward the broader use of this technology for functionalising surfaces at industrial scale. In this research, a green nanosecond laser was investigated for producing LIPSS on stainless steel under air and argon environments. The performance of LIPSS treatments in air was correlated to the light diffraction response of processed surfaces. In argon environment, the intensity of the diffracted light increased and this was indicative of the improved homogeneity of LIPSS generated on the surfaces. The relatively low-quality LIPSS produced in air can be attributed to the formation of oxides as a side effect compared to the laser processing in argon. These side-effects were confirmed by the conducted SEM, AFM and XPS analysis. The future research will be focused on correlating the wetting properties of dual-scale structures (LIPSS on top of microscale structures) and their dependance on processing conditions.

References

[1] C. Florian et al., "Surface functionalization by laser-induced periodic surface structures. Journal of Laser Applications," 32(2), p.022063, 2020.
[2] P. Nürnberger et al., "Orthogonally superimposed laser-induced periodic surface structures (LIPSS) upon nanosecond laser pulse irradiation of SiO2/Si layered systems," Applied Surface Science, vol. 425, pp. 682-688, 2017.
[3] T. Karkantonis et al., "Femtosecond laser-induced sub-micron and multi-scale topographies for durable lubricant impregnated surfaces for food packaging applications," Surface & Coatings Technology, vol. 399, p. 126166, 2020.
[4] R. Y. Siddiquie et al., "Anti-Biofouling Properties of Femtosecond Laser-Induced Submicron Topographies on Elastomeric Surfaces," Langmuir, vol. 36, no. 19, pp. 5349-5358, 2020.
[5] A. Gaddam et al., "Anti-icing properties of femtosecond laser-induced nano and multiscale topographies," Applied Surface Science, vol. 552, p. 149443, 2021.
[6] A. Batal et al., "Response of Saos-2 osteoblast-like cells to laser surface texturing, sandblasting and hydroxyapatite coating on CoCrMo alloy surfaces," Materials Science and Engineering: C, vol. 98, pp. 1005-1013, 2019.
[7] D. Bhaduri et al., "Laser polishing of 3D printed mesoscale components," Applied Surface Science, vol. 405, pp. 29-46, 2017.
[8] V. Vercillo et al., "Durability of superhydrophobic laser-treated metal surfaces under icing conditions," Materials Letters: X, vol. 3, p. 100021, 2019.
[9] J. S. Hwang et al., "Fabrication of printable nanograting using solution-based laser-induced periodic surface structure process," Applied Surface Science, vol. 547, p. 149178, 2021.
[10] P. Nürnberger et al., "Influence of substrate microcrystallinity on the orientation of laser-induced periodic surface structures," Journal of Applied Physics, vol. 118(13), p.134306, 2015.
[11] J. Simões et al., "High-speed Laser-Induced Periodic Surface Structures (LIPSS) generation on stainless steel surface using a nanosecond pulsed laser," Surface & Coatings Technology, vol. 344, pp. 423-432, 2018.
[12] J. M. Romano et al., "Triangular laser-induced submicron textures for functionalising stainless steel surfaces," Applied Surface Science, vol. 440, pp. 162-169, 2018.